The difficulties of simulating the acoustics of an empty rectangular room with an absorbing ceiling

Marbjerg, Gerd; Brunskog, Jonas; Jeong, Cheol-Ho

Published in:
Applied Acoustics

Link to article, DOI:
10.1016/j.apacoust.2018.06.017

Publication date:
2018

Document Version
Peer reviewed version

The difficulties of simulating the acoustics of an empty rectangular room with an absorbing ceiling

Gerd Marbjerg[a,1,*], Jonas Brunskog[b], Cheol-Ho Jeong[b]

[a] *Saint-Gobain Ecophon, 265 03 Hyllinge, Sweden*
[b] *Acoustic Technology, Department of Electrical Engineering, Technical University of Denmark, 2800 Kgs. Lyngby, Denmark*

Abstract

In this study, simulations of a scale model of an unfurnished rectangular room with an absorbing ceiling using an energy-based geometrical acoustic model and a phased geometrical acoustic model are compared to measurements. This room can represent a typical classroom or office. This comparison concluded that the phased model can capture more details of the sound field, particularly at low frequencies. For accurate predictions, precise surface descriptions are needed for the phased GA method, which are not always available. The main drawback of the phased model is a longer calculation time.

1. INTRODUCTION

Many common rooms, e.g. offices and classrooms, are rectangular with absorbing ceilings and low scattering on the surfaces. The sound fields in them are therefore highly non-diffuse, which can increase the need for precision in simulations of their acoustic properties. Many commonly used simulation tools for room acoustics are energy-based geometrical acoustic methods, which means that they neglect the wave nature of the sound propagation and thus phase information in the propagation and on reflections. Tracing the phase can be of particular importance when modeling the acoustics of a room below the Schroeder

*Corresponding author
Email address: jbr@elektro.dtu.dk (Jonas Brunskog)
[1] Current address: Acoustic Technology, Department of Electrical Engineering, Technical University of Denmark, 2800 Kgs. Lyngby, Denmark

frequency [1], where the modal overlap is low. The Schroeder frequency generally increases for a decrease in the size of a room, and phase information can therefore be especially important when simulating the acoustics of smaller rooms at low frequencies. It has furthermore been shown that the phase shifts on reflections can be important for surfaces of high absorption [2]. Improving the accuracy of geometrical acoustic simulations by use of pressure-based models with complex-valued and angle-dependent boundary conditions has previously been done in phased beam tracing [2, 3, 4, 5], phased ray-tracing [6] and also in the image source method [7, 8, 9]. The aim of the present study is to compare measurements of a scale model in two configurations with results from an energy-based simulation model and from a pressure-based simulation model.

The room acoustic simulation tool PARISM [10] (Phased Acoustical Radiosity and the Image Source Method) has been developed in order to be able to model the acoustics of rooms with non-diffuse sound fields and absorbing ceilings. PARISM is, as the name implies, a combination of the image source method (ISM) and acoustical radiosity (AR) that includes phase information in the propagation and on reflections in ISM by pressure-based summation of the reflections. It also includes the angle dependence of the absorbing surface properties in both ISM and in AR. PARISM is an extension of the energy-based CARISM [11] (Combined Acoustical Radiosity-Image Source Method). AR is inherently energy-based, but in PARISM a pressure impulse response is reconstructed. The result of PARISM is thus a pressure impulse response. The basic theory and algorithm of PARISM can be found in previous work by the authors [10, 12].

ODEON [13, 14, 15] is a well-established room acoustic simulation software that is based on a hybrid model, in which early reflections are found by a combination of ISM and ray tracing, and the late reflections are found by ray tracing. ODEON is energy-based and uses angle-independent diffuse field descriptors of the surface properties, but an approximated angle dependence can be included [16].

It has been shown that it is important to include surface scattering in geomet-

rical room acoustic simulation [17], and reflections are therefore often divided into two parts: a specular reflection and a scattered reflection. Both PARISM and ODEON include scattered reflections, but in quite different ways. It is however assumed that the same descriptor can be used in the two methods to determine the amount of sound energy scattered in a reflection.

The angle dependence of surface properties is in some geometrical methods completely disregarded, in some approximated [14, 16], and in some fully included [10]. The angle dependence of absorption properties is important in non-diffuse sound fields, because some angles of incidence are more likely to occur than others. It has been shown that the sound field of a rectangular room with an absorbing ceiling and low diffusion can be decomposed into two parts: the non-grazing sound field that has small angles of incidence with the absorbing ceiling and the grazing sound field that has large angles of incidence with the ceiling [18]. A porous absorber ceiling generally absorbs most efficiently at small angles of incidence, whereas the absorption coefficient approaches zero for grazing incidence [19]. The non-grazing sound field therefore decays much faster than the grazing. Including the angle dependence of the sound absorption of an absorbing ceiling can therefore be necessary to obtain acceptable simulation results.

In this study, PARISM simulations and ODEON simulations are compared with measurements to investigate the influence of including full angle dependence and phase information in geometrical acoustic simulations of non-diffuse sound fields. This will illustrate the difficulties in simulating rectangular rooms with absorbing ceilings and low scattering. When simulating real rooms and comparing with measurements, it is often a problem that the surface properties are not known but must be determined by rough measurements, numerical models, or estimated and fitted. This is the case in this study, which thus also illustrates the difficulties when using simulations in practice. The input surface descriptors to the two models are as much the same as possible, but some differences will occur due to the inherent differences in the models.

2. Surface properties

For room acoustic simulations, choosing the appropriate acoustic descriptors for the surfaces is important in order to get reliable results. The choice must be based on the room type, simulation method and surface materials. There are several descriptors that can be used, but often the choice is limited by the availability of the descriptors [20]. In geometrical room acoustic simulations, two properties of the surfaces are needed: their absorbing and their scattering characteristics. For the absorbing characteristics in energy-based simulation tools, the absorption coefficient is commonly used because it is the fraction of the energy incident on a surface that is absorbed. The absorption coefficient can be angle-dependent, but in many cases absorption coefficients are determined under assumed diffuse field conditions, e.g. according to ISO 354 [21]. This coefficient can be referred to as the Sabine absorption coefficient because it is calculated from Sabine's equation. Alternatively, a diffuse field absorption coefficient can be estimated from the angle-dependent absorption coefficient by use of Paris' law [22], which states that

$$\alpha_{RI} = \int_0^{\pi/2} \alpha(\theta) \sin(2\theta)\, d\theta, \tag{1}$$

where $\alpha(\theta)$ is the angle-dependent absorption coefficient, θ is the angle of incidence with the normal of the surface and the result, α_{RI}, is referred to as the random-incidence (RI) absorption coefficient.

Manufacturers of materials generally only supply the Sabine absorption because it is easy to measure and simple to understand for the users. Measurements of the Sabine absorption coefficient can give values that are larger than one, which does not physically make sense for the common definition of the absorption coefficient as used in geometrical acoustic software, because it is not possible that more energy is absorbed than what is incident on the absorber. The assumptions of the determination of the Sabine absorption coefficient are however only valid for an infinite absorber and the finite size of the absorber and diffraction from the edges can thus result in values above one. Thomasson's size

correction [23] can be applied to approximate the equivalent infinite RI absorption coefficient. However, the absorption coefficients given by manufacturers are often what can be referred to as practical absorption coefficients for which any values above one are simply truncated to one [24].

Rindel has developed a method for estimating an angle-dependent absorption coefficient from a diffuse field absorption coefficient [16]. This method assumes that the diffuse field absorption coefficient is equal to the absorption coefficient at 60° for local reaction, and from this an angle-dependent absorption coefficient is calculated. It has been shown that the local reaction assumption can be problematic for absorbers with an air gap [25] and that the equivalent incidence angle of a porous absorber in a diffuse sound field is 45° if it is of extended reaction and 55° if it is of local reaction [26]. The approximated angle dependence is thus not complete, but in many practical applications it can be useful if the only available value is a diffuse field absorption coefficient, because an estimated angle dependence is then expected to be better than none.

If the phase shifts on reflections are to be included in the simulations, it is not possible to use the absorption coefficient to describe the absorbing characteristics of the surfaces. Complex-valued descriptors, such as the reflection factor R or the surface impedance Z, must then be used. For plane waves incident on an infinite absorber, the absorption coefficient is related with the reflection factor by $\alpha = 1 - |R|^2$. The reflection factor can for plane waves be found from the impedance by

$$R(\theta, f) = \frac{Z(\theta, f) - \rho_0 c_0 / \cos\theta}{Z(\theta, f) + \rho_0 c_0 / \cos\theta}, \tag{2}$$

where ρ_0 is the density of air and c_0 is the speed of sound in air. In the above equation, it is assumed that the impedance depends on angle of incidence, and materials for which this is the case are said to be of extended reaction. If it instead is assumed that the impedance is angle-independent, such that normal incidence impedance is sufficient for describing its behavior, the material is said to be of local reaction.

The angle-dependent impedance is rarely available, because it can be prob-

lematic to measure, especially for high angles of incidence and small samples [27, 28]. It can therefore be necessary to use models for the estimation of it. One such model is Miki's model [29] that uses the flow resistivity of a porous absorber to estimate the impedance. The flow resistivity is much more practical to measure than an angle-dependent impedance. Gunnarsdóttir et al. [25] have shown that for a porous absorber with rigid backing, Miki's model produces acceptable results, regardless of whether local or extended reaction is assumed. For a porous absorber with an air gap backing, it was found that Miki's model can also produce acceptable results as long as extended reaction is considered [19]. A misprint has been found in the work by Gunnarsdóttir et al. [25], where the k_0 in Eq. (2) should be k.

The scattering characteristics are most often described by the scattering coefficient, which is the fraction that is non-specularly reflected to the total reflected energy [30]. The scattering coefficient therefore does not contain any information about the angular pattern in which the scattered energy is distributed. The scattering coefficient can be measured under assumed diffuse field conditions following the ISO 17497-1 [31], giving a result that is independent of the angle of incidence, and this value is therefore referred to as the random-incidence scattering coefficient. To include the full distribution patterns of the scattered reflections, bidirectional reflectance distribution functions (BRDF's) [32] must be used, which are dependent on both the angle of incidence and the outgoing angle. The BRDF's are however rarely used in geometrical acoustics because it would complicate the calculations, and for simplicity the random-incidence scattering coefficient is thus the preferred choice. Unlike the random-incidence scattering coefficient, BRDF's are furthermore difficult to measure, and the random-incidence scattering coefficient is therefore also more often available.

The random-incidence scattering coefficient is rarely known for materials that are not designed with the specific purpose of scattering sound and must for many common surfaces be estimated based on experience. For rooms with non-diffuse sound field, scattering has a large influence [33] and setting the correct scattering coefficient can therefore be a crucial factor in obtaining good

simulation results.

3. Method

Simulated results from the geometrical acoustic tools ODEON and PARISM are compared with measured results to exemplify the effects of angle dependence and phase in a rectangular room with an absorbing ceiling. This section describes how the measurements and simulations were carried out.

3.1. The test room and the measurements

The room used for measurements is a scale model of a rectangular room with an absorbing ceiling. It is a chipboard (22 mm thickness) box with very little surface irregularities, and it has dimensions [1.57 x 1.25 x 1] m. It can thus be seen as a 1:5 scale model of a classroom with a very high ceiling height or a 1:3 scale model of a small office. Regardless, no rescaling is done as the simulations are done with the same dimensions to avoid errors in such processing. The frequency range of interest is however shifted slightly upwards compared to what is normally regarded in room acoustics, and thus includes the 250 Hz to 16 kHz octave bands. The sampling frequency of the measurements and of the PARISM simulations is 48 kHz. In ODEON it is not possible to change the frequency range, and the 250 Hz to 8 kHz octave bands therefore limit the comparison with the ODEON simulations.

The absorption coefficients of the walls and floor are determined from reverberation time measurements in the room before the absorbing ceiling was installed. All surfaces are then of the same material and since they are relatively acoustically rigid, it is assumed that the sound field in the room is diffuse enough to apply Sabine's equation to determine an average absorption coefficient, α_{av}, which is given in Table 1. The source was placed in a corner pointing towards the diagonally opposite corner and 6 receiver positions were used. Air absorption determined according to ISO 9631 [34] was included in the calculations.

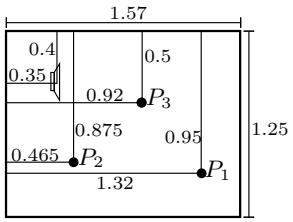

Figure 1: Source and receiver positions, P_1, P_2 and P_3, in the scale model with all distances in m. The height of all receiver postions is 0.24 m, and the height of the source is 0.3 m.

Table 1: The input data for the simulations. α_{av} is the **measured** average Sabine absorption coefficient that is used for the walls and floor in all simulations, α_{ceil} is the random incidence absorption coefficient of the ceiling **based on numerical simulations with Miki's model [29] and Eq. (1)**, α_{sin} is the **measured** Sabine absorption coefficient of the diffuser, s_w is the scattering coefficient of the walls **determined by estimation and fitting**, s_c is the scattering coefficient of the ceiling and the floor **determined by estimation**, and s_{sin} is the **measured** random-incidence scattering coefficient of the diffuser.

f [Hz]	250	500	1 k	2 k	4 k	8 k	16 k
α_{av}	0.032	0.033	0.034	0.038	0.038	0.035	0.035
α_{ceil}	0.409	0.682	0.830	0.792	0.886	0.928	0.938
α_{sin}	0.100	0.217	0.179	0.076	0.049	0.096	0.071
s_w	0.04	0.04	0.04	0.04	0.05	0.05	0.05
s_c	0.01	0.01	0.01	0.01	0.01	0.01	0.01
s_{sin}	0.038	0.076	0.167	0.404	0.509	0.592	0.633

Figure 2: Picture of the scale model with the absorbing ceiling and the sinusoidal diffuser in the vertical orientation.

The room has been fitted with a porous absorber ceiling of 15 mm thickness with an 85 mm air gap behind it, see Fig. 2, which gives a resulting height of 0.9 m. The flow resistivity of the porous absorber is 77.8 $\frac{kPa\ s}{m^2}$ measured according to NF EN 29053 [35]. The characteristic impedance and the propagation constant of the porous medium are calculated using Miki's model [29]. From these, the surface impedance is calculated by Eq. (2) in Ref. [25]. The magnitude and phase angle of the reflection factor at 0°, 45° and 80° are shown in Fig. 3, from which it can be seen that the absorption of the ceiling is much lower at high angles of incidence. The random incidence absorption coefficient calculated with Eq.(1) is shown in the lower part of Fig. 3. The octave band values of the random incidence absorption coefficient of the ceiling are denoted α_{ceil} and seen in Table 1. In the rest of this paper, the room with only the absorbing ceiling will be referred to as the empty room.

After measurements in the empty room, the surface scattering is increased by introducing a circular diffuser with a sinusoidal pattern. It is 3.7 cm thick in total, of a material that is 2 mm thick and has a diameter of 80 cm, which gives an area of 0.5 m^2. The period of the sinusoidal pattern is 10 cm. The diffuser can be seen on the left wall of the room in Fig. 2. The measurements

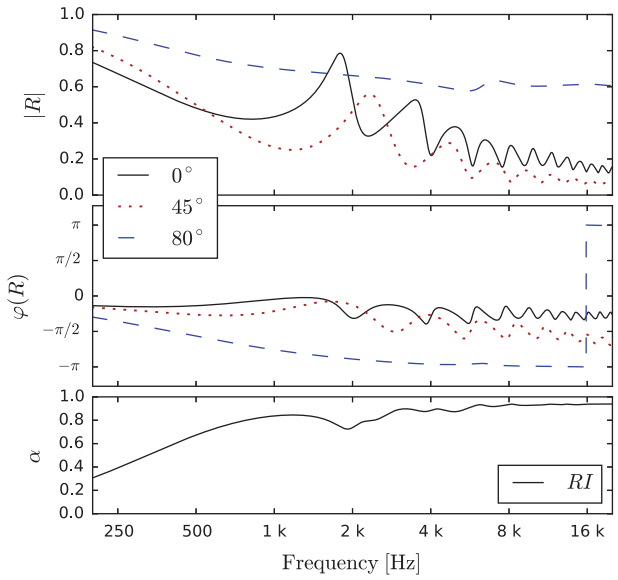

Figure 3: **Above and centre:** Reflection factor of the porous absorber ceiling calculated with Miki's model at 0° (*black solid line*), 45° (*red dotted line*) and 80° (*blue dashed line*). **Above:** Magnitude of the reflection factor. **Centre:** Phase angle of the reflection factor. **Below:** Random incidence absorption coefficient of the ceiling.

were done with two orientations of the diffuser: vertical and horizontal, and in Fig. 2 the diffuser is seen in the vertical orientation. The scattering coefficient of the diffuser has been measured following ISO standard 17497-1 [31], thus under assumed diffuse field conditions. The scattering coefficient of the diffuser is denoted s_{sin} in Table 1. The Sabine absorption coefficient of the diffuser has been measured following ISO standard 354 [21], but no information about the angle dependence of or phase shifts on reflections from the diffuser was available. The absorption coefficient is denoted α_{sin} and is stated in Table 1. For measurements of the scattering and absorption coefficients of the diffuser, the empty room without the absorbing ceiling was used. Panel diffusers were added to make it more similar to a scaled reverberation chamber, which is shown in Fig. 4.

Figure 4: Picture of the scale model as an approximated reverberation chamber, thus without the absorbing ceiling and with added panel diffusers.

The measurements of the scattering and absorption coefficients of the diffuser, and of the absorption coefficient of the chipboard were, as mentioned, done with a loudspeaker placed in a corner of the room pointing towards the diagonally opposite corner. The room acoustical measurements were done with the same loudspeaker, but it was then placed on a stand in a height of 0.3 m and the orientation that is seen in Figs. 1 and 2. The loudspeaker used for all measurements was a Vifa (XT25TG30-04) tweeter loudspeaker. In standard room acoustical measurements, an omnidirectional source should be used, but no om-

nidirectional source suitable for the scale model was available. The phased free field directivity of the loudspeaker has been measured, which can be used for the simulations, see Fig. 6. Rotational symmetry is assumed for the loudspeaker and the directivity was therefore only measured on a single plane. The frequency response was measured at 5 degree intervals from 0 to 25.6 kHz with a resolution of 4 Hz. When the directivity of the loudspeaker is included in the PARISM simulations, the inverse Fourier transform is taken. This introduced some noise in the tail of the impulse response of the loudspeaker, and it was found that this noise could influence the resulting simulated reverberation time. Inverse Fourier transform was therefore applied to the frequency responses of the loudspeaker to obtain impulse responses. A half Hamming window was then applied to the loudspeaker impulse responses to eliminate the noise. Fourier transform was then applied to get back to frequency responses that were used for the ISM simulations. The signal-to-noise ratios of the impulse responses of the loudspeaker are estimated by assuming that the first 0.1 s of an impulse response is signal and the final 0.15 s is noise. This is an approximate approach, but the best that can be done with the current data. The signal-to-noise ratio as a function of the angle is seen in the Fig. 5. The calculation is done for the impulse responses with and without the window applied. It is seen that the signal-to-noise ratio is above 35 dB for the windowed directivity impulse responses for all angles.

The same microphone, a 1/4 inch 4136 Brüel & Kjær, was used for all measurements. For the room acoustical measurements, it was placed in the positions as can be seen in Fig. 1 and in a height of 0.24 m.

Based on the measured reverberation times, the Schroeder frequency of the empty room with the absorbing ceiling is around 1 kHz, and with the absorbing ceiling and the diffuser it is around 900 Hz.

3.2. PARISM simulations

The scattering coefficients of the walls, floor and ceiling are not known and near impossible to measure, and they must therefore be estimated based on experience. It is common that the scattering coefficients of smooth surfaces

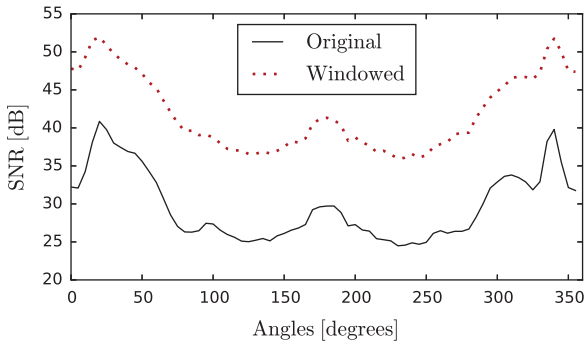

Figure 5: Signal-to-noise ratios of the directivity impulse responses of the loudspeaker.

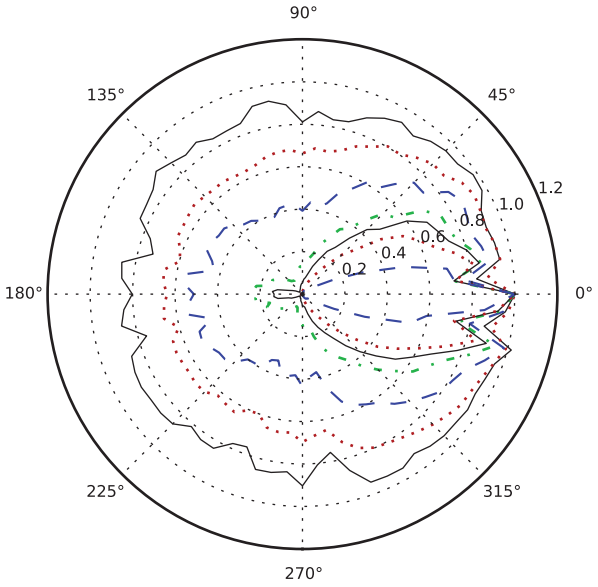

Figure 6: Polar plot of the directivity of the loudspeaker normalized by the response at 0°. *Solid black lines:* 250 Hz and 4 kHz, *Red dotted lines:* 500 Hz and 8 kHz, *Blue dashed lines:* 1 kHz and 16 kHz, *Green dashed-dotted line:* 2 kHz.

are unknown, but recommended values are in the range 0.01 to 0.05 [15]. The scattering coefficients of the ceiling and the floor, denoted s_c in Table 1, are set to 0.01 for all frequencies. For the walls, it was initially set to 0.04 for all frequency bands and the frequency dependence was then altered such that the simulated PARISM decay curves fit the measured ones best possible for the empty room with the absorbing ceiling. This method is in the rest of this paper referred to as estimation and fitting of the scattering coefficient. The resulting values can be seen as s_w in Table 1, and it should be noted that the fitting that was done did not change the values much from the initial 0.04. For ISM, linear interpolation is used on the octave band values of the scattering coefficients to obtain values for the full frequency range.

In the simulations, all surfaces must be defined as polygons. Though it is possible to approximate a circle by several polygons, it has been chosen to represent the scatterer as a square to reduce the calculation complexity. The surface area of the square should be the same as the circle, which makes each side of the square 0.71 m.

For the ISM, the complex-valued reflection factor of the ceiling, as shown in Fig. 3, is used. For AR, the angle-dependent absorption coefficient calculated from the reflection factor is used. The walls and the floor are quite rigid and it is assumed that they do not cause any phase shifts on reflections such that they can be described by absorption coefficients, thus α_{av} in Table 1. The absorption of the sinusoidal diffuser is described by its measured Sabine absorption coefficient, α_{sin}. For ISM, linear interpolation is used on the octave band absorption coefficients to obtain values for the full frequency range. The reflection factor is then found as $R = \sqrt{1-\alpha}$.

The directivity of the source is included in the simulations by multiplying the source factor of each image source with the phased frequency response corresponding to the direction from which the sound is emitted from the source. It is assumed that the directivity is rotationally symmetric around the normal axis of the loudspeaker, such that only the angle with the normal is determined. The result of ISM is a frequency response to which inverse Fourier transform is

applied to obtain an impulse response.

The termination of the ISM is adaptive in PARISM, which means that an image source is not produced if its potential contribution is small compared to that from radiosity. Therefore, the radiation density from ISM at the reflecting surface must be above a certain fraction of the radiation density received at that surface from other AR elements in the same reflection order. If the image sources are terminated too quickly, AR will be dominant too soon in the decay making the sound field more diffuse. This will often be seen as an increase in the slope of the decay curves, and to determine whether the fraction has been set sufficiently low, the decay curves must be checked. By regarding the simulated decay curves, it was found that for the present room, the fraction had to be low such that many image sources are included. The fraction was set to 0.05 (-13 dB), meaning that the energy from radiosity had to be 20 times higher than the energy from ISM in order to terminate that line of image sources. Because PARISM calculates all octave bands simultaneously, this criterion should be satisfied for all bands at once before an image source is terminated.

As mentioned in the introduction, the result of AR is an energy impulse response and a stochastic method is used to reconstruct a pressure impulse response. In the previous work [10], three methods are given for this. One of them gives an estimate of the ensemble mean of the squared absolute impulse response, which is recommended to use when room acoustic energy parameters such as reverberation time are to be calculated. The two other methods reconstruct the pressure impulse responses by use of noise signals, and the difference between these methods is whether the noise signal is Gaussian noise or a signal of random -1 or 1. Due to the randomness in these noise signals, repeating the realization of the reconstructions will give slightly different results. In the present investigation, all decay curves and room acoustical parameters are found from the ensemble mean of the squared absolute pressure impulse response, but the frequency responses are calculated using one sample of the Gaussian noise signal.

3.3. Angle-independent PARISM

A PARISM simulation was also done where the angle dependence and phase shifts on reflections from the ceiling are disregarded. The absorption properties of the ceiling are thus described by the random incidence absorption coefficient as shown in the lower part of Fig. 3. The implementation of ISM in PARISM is still pressure-based, not energy-based. PARISM simulations with angle-independent and real-valued boundary conditions therefore differ from CARISM [11] simulations by the fact that ISM in PARISM is implemented as summation of pressure in the frequency domain, thus including interference between reflections [2]. The frequency domain implementation furthermore include smearing of impulses in time due to filtering [36]. These PARISM simulations with the random incidence absorption coefficient are hereafter referred to as PARISM RI.

3.4. ODEON

As described in the introduction, diffuse field absorption coefficients should be the input to ODEON, but an angle dependence is estimated for soft surfaces [16]. This option can be deselected, and simulations without the angle dependence in ODEON are therefore also done for comparison.

All surface reflections in ODEON result in a single ray, and scattering is considered by weighting the specular direction and a random scattered direction by means of the scattering coefficient. The random scattered direction is found by the method of oblique Lambert [15]. Only a single value scattering coefficient can be set for each surface in ODEON, so the frequency dependence cannot be chosen freely, as in PARISM, but will follow a predefined curve. The same fitting of the scattering coefficient, as done for PARISM, is therefore not possible in ODEON. Examples of the scattering coefficient curves can be found in section 6.4 of the manual of ODEON [14]. The manual recommends setting the scattering coefficient equal to that of a mid-frequency value, and the mean of the 500 Hz and 1 kHz octave bands is a suggested choice. It was attempted to keep the input to PARISM and ODEON as much the same as possible when choosing

the scattering coefficients for ODEON. Looking at the scattering coefficient for the sinusoidal diffuser in Table 1 this would be 0.12, but when looking at the frequency curves in the ODEON manual it is seen that the curve for a scattering coefficient of around 0.1 will not be steep enough to give a high enough scattering coefficient at higher frequencies. The curve of a mid-frequency scattering coefficient of 0.25 seemed to be a better fit the actual scattering coefficient of the diffuser as it is just over 0.5 at 8 kHz. 0.25 was therefore the chosen value set in ODEON. The scattering coefficients of the ceiling and floor were set to 0.01 and those of the walls were set to 0.04.

The number of late rays in ODEON was increased from the standard settings to 16000, the maximum reflection order to 2000, the transition order from early to late reflections to 3 and the number of early rays to 4000. The number of late rays and the transition order are higher than the recommended. This was chosen because it is expected to be challenging to model the acoustics of the scale model because of its very non-diffuse sound field.

In ODEON, a directivity pattern can be defined in octave bands with a 10 degree resolution of the azimuth and elevation angle. As in PARISM, rotational symmetry around the normal axis of the loudspeaker was assumed.

3.5. Overview of the input to PARISM and ODEON

Table 2 summarizes how the absorption and scattering of the surfaces are described in the three simulation methods.

4. Results and analysis

In this section, the measured and simulated results are presented; first by showing parameters regarding the reverberation and the speech intelligibility, next by comparing the decay curves and frequency responses of PARISM with those of the measurements. Lastly, a single reflection from the ceiling is regarded using different surface descriptors.

Table 2: An overview of the input that is used for the simulations. It should be noted that the scattering coefficients for ODEON are mid-frequency values, and that their frequency dependence is predefined by ODEON.

	Full PARISM	PARISM RI	ODEON
Ceiling abs.	Refl. factor, Fig. 3	RI abs. coef., Fig. 3	α_{ceil} Table 1
Ceiling + floor scat.	s_c, Table 1	s_c, Table 1	0.01
Wall + floor abs.	α_{av}, Table 1	α_{av}, Table 1	α_{av}, Table 1
Wall scat.	s_w, Table 1	s_w, Table 1	0.04
Diffuser abs.	α_{sin}, Table 1	α_{sin}, Table 1	α_{sin}, Table 1
Diffuser scat.	s_{sin}, Table 1	s_{sin}, Table 1	0.25

4.1. Reverberation and speech intelligibility

The results from the measurements and the simulations are first regarded in terms of the room acoustic parameters reverberation time (T_{30}), early decay time (EDT) and definition (D_{50}) as defined by ISO 3382-1 [37]. D_{50} is chosen because it is a measure of the speech intelligibility, which is often important in the regarded room type. The spatial means and spatial standard deviations are calculated from the three receiver positions, and the results are shown in Figs. 7 and 8. The first impression is that none of the simulation results match the measurements very well, but PARISM matches the frequency dependence of the parameters that is seen in the measurements better. The reverberation time and early decay time are underestimated by the full PARISM in the 1 kHz and 2 kHz bands.

Looking at the right sides of Figs. 7 and 8, it is seen that the ODEON results above 250 Hz, unlike the measurements, are almost frequency-independent. Since ODEON does not include the phase information and thus not wave interference and modal behaviour, any frequency dependence must come from the input data. Regarding the absorption coefficients α_{av}, α_{ceil} and α_{sin} in Table 1, it is seen that α_{av} and α_{sin} do not vary much over frequencies. The lack of phase information in ODEON can also be seen by the much smaller spatial standard deviation. It must therefore be concluded that if details of the sound field in a

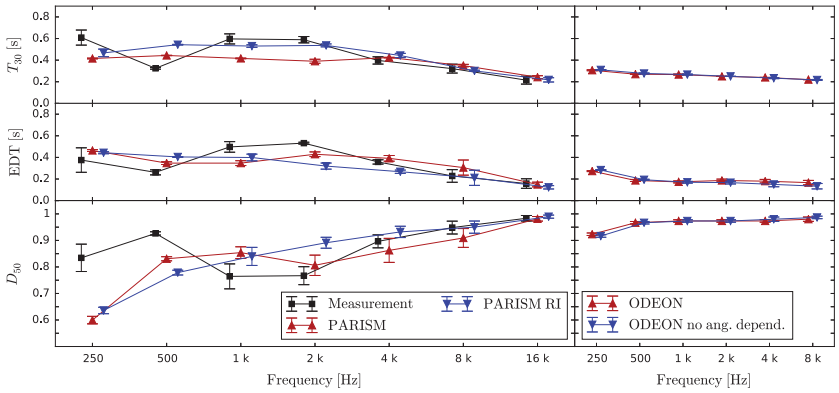

Figure 7: Spatial means and spatial standard deviations of the measured and simulated room acoustical parameters in the empty room of which the Schroeder frequency is around 1 kHz. PARISM RI refers to PARISM with random incidence absorption coefficient for the ceiling.

room of the present type are to be simulated, energy-based geometrical models are insufficient. The values predicted by ODEON seem to converge with the measured values at high frequencies, which confirms that energy-based methods can be useful for predicting the acoustic behaviour of rooms at frequencies well above the Schroeder frequency.

Regarding the ODEON simulations with and without the estimated angle dependence of the absorption of the ceiling in Figs. 7 and 8, it is seen that the differences are small. It is thus concluded that for the absorbing ceiling in the present case the estimated angle dependence does not have much influence.

In ISO 3382-1 [37], the subjective just noticeable difference (JND) for EDT is stated as 5 % and for D_{50} it is stated as 0.05. The errors of the simulations with reference to the measurements and normalised by the JNDs are calculated with the errors functions defined as follows

$$\begin{aligned} \epsilon_{T_{30}} &= \frac{T_{30,sim}-T_{30,meas}}{T_{30,meas}} \frac{100\%}{5\%} \text{ [JNDs]} \\ \epsilon_{EDT} &= \frac{EDT_{sim}-EDT_{meas}}{EDT_{meas}} \frac{100\%}{5\%} \text{ [JNDs]} \\ \epsilon_{D_{50}} &= (D_{50,sim} - D_{50,meas}) \frac{1}{0.05} \text{ [JNDs]}, \end{aligned} \tag{3}$$

where subscript *sim* refers to the simulated values and subscript *meas* refers

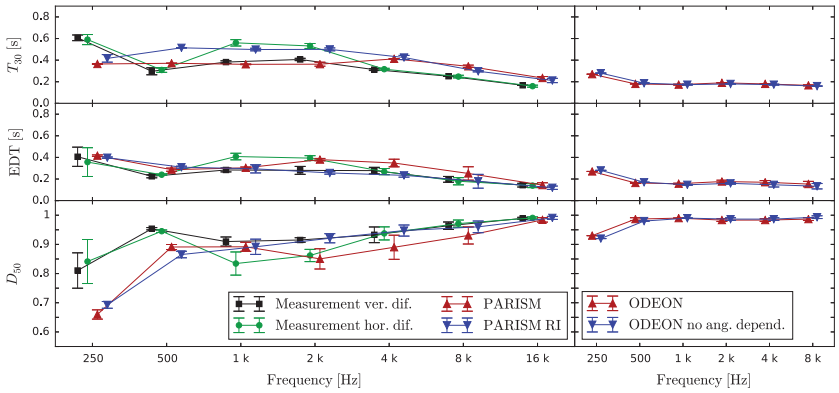

Figure 8: Spatial means and spatial standard deviations of the measured and simulated room acoustical parameters in the room with the diffuser of which the Schroeder frequency is around 900 Hz. PARISM RI refers to PARISM with random incidence absorption coefficient for the ceiling.

to the measured ones. Because the measurement results with the sinusoidal diffuser depend on the orientation of the diffuser, the errors are calculated with respect to an average of the results from the two orientations. The errors are shown in Table 3. It is seen that the errors of the PARISM simulations exceed the JND for most frequencies and configurations. For ODEON, nearly all errors exceed one JND. The parameter, for which most errors are less than one JND, is D_{50}. For the PARISM simulations, most errors from 500 Hz and up are actually below or only just above one JND, which indicates that the speech intelligibility is well predicted by this simulation.

The scientific foundation of the just noticeable differences stated in the standard is however not clear. Studies have been done [38, 39, 40, 41] that try to set the JND for the room acoustical parameters, but the conclusions are not clear. It can for instance be questioned how the type of sound influences the perceived reverberation and whether the values should be frequency-independent [38]. In the standard, the just noticeable difference for D_{50} is stated as being constant regardless of the size of D_{50}, but it has been shown that the perceivable change in D_{50} might depend on the value [39]. The just noticeable differences should

thus not be taken as the absolute truth.

The errors of the early decay time and reverberation time are calculated as relative errors, because this is how the JND is stated in the standard. For the frequency bands where the measured values are low, this gives some very large errors. This is for instance the case for the early decay time and the reverberation time at 16 kHz. However, regarding Figs. 7 and 8, the fit does not look quite as bad for PARISM as the errors indicate, especially for T_{30}.

Looking at Fig. 8 and comparing with Fig. 7, it is seen that the diffuser affects the sound field more when it is in the horisontal orientation than when it is in the vertical orientation at 1 kHz and 2 kHz. To quantify how much the diffuser changes the room acoustical parameters, the difference between the measurements and simulations with and without the diffuser is calculated. The differences are quantified by $d_{T_{30}}$, d_{EDT} and $d_{D_{50}}$, which have been calculated by

$$\begin{aligned} d_{T_{30}} &= \tfrac{T_{30,dif}-T_{30,emp}}{T_{30,emp}} \, \tfrac{100\%}{5\%} \, [\text{JNDs}] \\ d_{EDT} &= \tfrac{EDT_{dif}-EDT_{emp}}{EDT_{emp}} \, \tfrac{100\%}{5\%} \, [\text{JNDs}] \\ d_{D_{50}} &= (D_{50,dif} - D_{50,emp}) \, \tfrac{1}{0.05} \, [\text{JNDs}], \end{aligned} \tag{4}$$

where subscript dif refers to the parameters with the diffuser included and subscript emp refers to the parameters without the diffuser. The differences are presented in Table 4. When looking at the measurements, it is seen that the parameters are changed more by the diffuser in the vertical orientation than by the diffuser in the horisontal orientation. In the vertical orientation, the early decay time is for instance reduced by up to 9.5 JNDs, whereas the maximum reduction by the diffuser in the horisontal orientation is 5.2 JNDs. The reverberation time is often less sensitive to small changes in the sound field, but here a clear difference is also seen. The maximum reduction of the reverberation time is 7.2 JNDs with the vertical diffuser, which is found in the 1 kHz octave band. In the same octave band the difference caused by the horisontal diffuser is only 1.2 JNDs. This indicates that turning the diffuser 90° creates a perceivable difference in the reverberation. In the simulations,

Table 3: Errors of the simulations. The errors are presented as number of JNDs. PARISM RI refers to the PARISM simulations with the random incidence absorption coefficient of the ceiling.

f [Hz]	250	500	1 k	2 k	4 k	8 k	16 k
	PARISM, empty						
$\epsilon_{T_{30}}$ [JNDs]	-6.4	7.3	-6.0	-6.8	1.3	1.8	2.6
ϵ_{EDT} [JNDs]	4.7	6.5	-6.0	-3.9	1.9	6.8	-1.1
$\epsilon_{D_{50}}$ [JNDs]	-4.7	-1.9	1.8	0.8	-0.7	-0.7	-0.0
	PARISM, with diffuser						
$\epsilon_{T_{30}}$ [JNDs]	-7.8	4.5	-4.7	-4.5	6.2	7.5	8.7
ϵ_{EDT} [JNDs]	1.8	4.6	-2.4	2.5	5.5	6.7	0.3
$\epsilon_{D_{50}}$ [JNDs]	-3.3	-1.1	0.4	-0.8	-0.9	-0.7	-0.1
	PARISM RI, empty						
$\epsilon_{T_{30}}$ [JNDs]	-4.7	13.5	-2.2	-1.8	2.3	-1.3	0.3
ϵ_{EDT} [JNDs]	3.6	10.9	-3.9	-8.0	-5.1	-1.5	-4.3
$\epsilon_{D_{50}}$[JNDs]	-4.0	-3.0	1.5	2.5	0.7	0.0	0.1
	PARISM RI, with diffuser						
$\epsilon_{T_{30}}$ [JNDs]	-6.1	13.9	1.2	1.3	7.0	3.8	5.9
ϵ_{EDT} [JNDs]	0.9	6.6	-3.0	-4.8	-2.9	-1.0	-3.1
$\epsilon_{D_{50}}$ [JNDs]	-2.7	-1.7	0.4	0.7	0.2	-0.1	0.0
	ODEON, empty						
$\epsilon_{T_{30}}$ [JNDs]	-9.9	-3.3	-11.1	-11.5	-7.9	-6.3	
ϵ_{EDT} [JNDs]	-5.4	-5.7	-13.0	-13.0	-9.9	-5.4	
$\epsilon_{D_{50}}$ [JNDs]	1.8	0.8	4.2	4.1	1.5	0.6	
	ODEON, with diffuser						
$\epsilon_{T_{30}}$ [JNDs]	-11.0	-8.1	-12.6	-11.9	-8.5	-6.6	
ϵ_{EDT} [JNDs]	-5.8	-5.9	-10.9	-9.5	-7.6	-3.7	
$\epsilon_{D_{50}}$ [JNDs]	2.1	0.7	2.4	1.9	1.0	0.4	

the diffuser is however described by a random incidence scattering coefficient, which has been measured under the assumption of a diffuse sound field. It must therefore be concluded that this measurement method does not always produce data that is sufficiently detailed for simulations of non-diffuse sound fields. The measured difference in the parameters when turning the diffuser should thus be taken into consideration when the simulation errors are regarded.

The differences in the parameters of the PARISM simulations with and without the diffuser are smaller than the difference in the measured parameters. Especially T_{30} that is reduced by around 4 or 5 JNDs at high frequencies in the measurements is not affected enough by the introduction of the diffuser in the PARISM simulations. The PARISM early decay times are more influenced by the diffuser than the reverberation times. This means that it is especially the late part of the decay that is not sufficiently influenced. In Fig. 7, it is seen that for the empty room, the T_{30} predicted by PARISM is too low at 1 kHz and 2 kHz, indicating that diffuseness of the empty room is overestimated at these frequencies by PARISM. The problem with the diffuseness in the late decay could be due to the fact that the late part is dominated by acoustical radiosity, which means that the sound field is more diffuse than the actual one. With the adaptive termination of image sources in PARISM, there is a risk of terminating image sources too quickly. When a family of image sources is terminated, all the energy will thereafter be reflected diffusely by AR, because diffuse-to-specular reflections are not allowed in PARISM. When all image sources are terminated, all reflections are diffuse and the increase in the diffusivity of the sound field is thereafter minimal. Even after the diffuser is introduced in the room, it must be said that the total surface scattering is low in the room. The scattering is furthermore concentrated on a small part of the surface area and only on a single surface, so many reflections will not be influenced by the diffuser. It is therefore expected that the diffuseness of the room gradually increases throughout the decay. If the termination of the image sources in PARISM is done too quickly, the simulations will not behave like this. In Sec. 4.2, decay curves will be evaluated with a higher number of image sources to test the influence of the

Table 4: Differences between the measurements and the simulations with and without the diffuser as defined by Eq. (4). The differences are presented as number of JNDs.

f [Hz]	250	500	1 k	2 k	4 k	8 k	16 k
	PARISM						
$d_{T_{30}}$ [JNDs]	-2.5	-3.3	-2.6	-1.4	-0.6	-0.4	-0.6
d_{EDT} [JNDs]	-2.1	-3.5	-2.5	-2.3	-2.2	-3.5	-0.7
$d_{D_{50}}$ [JNDs]	1.2	1.2	0.8	0.9	0.6	0.4	0.1
	ODEON						
$d_{T_{30}}$ [JNDs]	-2.4	-6.7	-7.0	-4.8	-5	-4.8	
d_{EDT} [JNDs]	-0.2	-2.5	-1.9	-1.1	-1.1	-1.6	
$d_{D_{50}}$ [JNDs]	0.1	0.4	0.3	0.2	0.2	0.1	
	Measurements, vertical diffuser						
$d_{T_{30}}$ [JNDs]	-0.07	-1.7	-7.2	-6.2	-4.3	-4.4	-4.4
d_{EDT} [JNDs]	1.6	-2.8	-8.6	-9.5	-4.5	-2.7	-1.9
$d_{D_{50}}$ [JNDs]	-0.5	0.5	2.9	3.0	0.7	0.3	0.1
	Measurements, horisontal diffuser						
$d_{T_{30}}$ [JNDs]	-0.6	-0.9	-1.2	-2.0	-4.1	-4.6	-5.2
d_{EDT} [JNDs]	-1.0	-1.7	-3.6	-5.2	-5.0	-4.3	-2.4
$d_{D_{50}}$ [JNDs]	0.1	0.4	1.4	1.9	0.8	0.5	0.1

termination.

The reverberation time simulated by ODEON is much influenced by the introduction of the diffuser, see Table 4. The influence is however not as frequency-dependent as it is in the measured results. Especially the large reduction of the reverberation time at low frequencies does not match with the measurements.

4.2. The decay curves

To have a look at the details of the behaviour of the PARISM simulations with different surface descriptions, the decay curves for receiver position P_1 are plotted for the empty room in Fig. 9. The full PARISM decay curves at 2 kHz, 4 kHz and 8 kHz are more linear than the PARISM RI decays that are more bent

curves. More linear decay curves indicate that the sound field is more diffuse. What could cause this difference in diffuseness will be further investigated in Sec. 4.4. At 500 Hz and 1 kHz, the full PARISM decays are faster but not more linear, and at 1 kHz the full PARISM decay deviates from the measured decay. This deviation will be regarded in the following by increasing the number of included image sources.

In the simulations for the full PARISM simulations in P_1 as shown in Fig. 9, 502528 image sources were included, and to see whether this was enough to obtain good results the energy fraction of the termination criterion of an image source was changed from 0.05 (-13 dB) to 0.017 (-18 dB). This simulation has a long calculation time and was therefore only done for receiver position P_1. The number of included image sources was then 1120305. Fig. 10 shows that for 2 kHz the higher number of image sources makes the PARISM decay curves match the measured decay curves better. For 1 kHz there is a very small improvement. With the increase in image sources, it is seen that for 1 kHz and 2 kHz, the slopes of the early parts of the decays become less steep. This indicates that the image sources are terminated too quickly such that the early reflections become overly diffuse. It could be that decreasing the termination criterion further such that even more image sources were included would improve the results, but that is simply to computationally heavy to test with the computer available for the present investigation.

4.3. Frequency responses

The frequency responses below the Schroeder frequency of the empty room from the measurements and from PARISM are shown in Fig. 11. ODEON does not calculate full frequency responses and is therefore not included in this comparison. The simulations with the low termination criterion (0.017) for the image sources are used, because this should give the most correct frequency responses. Both measured and simulated frequency responses have been normalized by the maximum values to make the amplitudes comparable. The frequency response of the ISM part of PARISM is also shown, because it is only

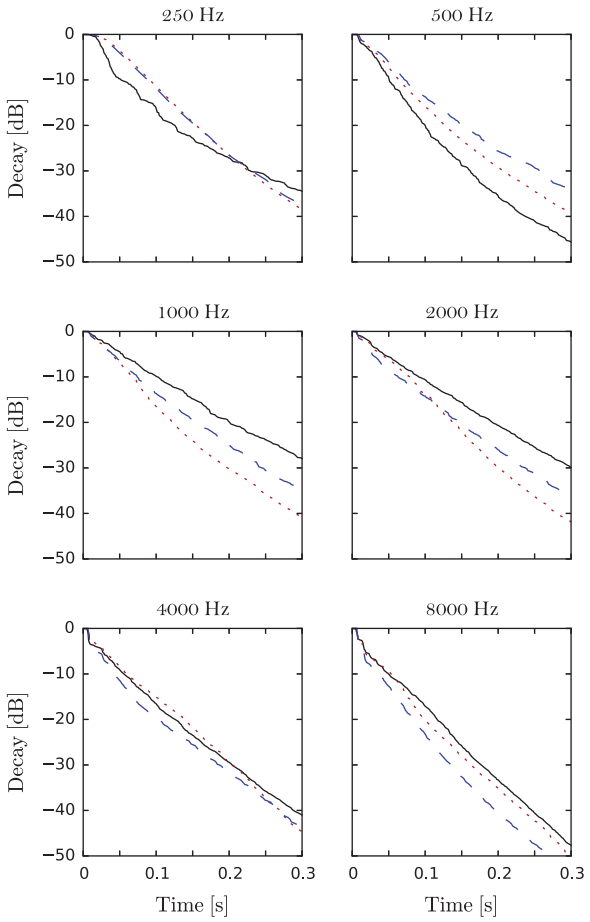

Figure 9: Decays of the empty room in receiver point P_1. *Solid black line:* Measurement, *Dotted red line:* full PARISM, *Dashed blue line:* PARISM with random incidence absorption coefficient of ceiling.

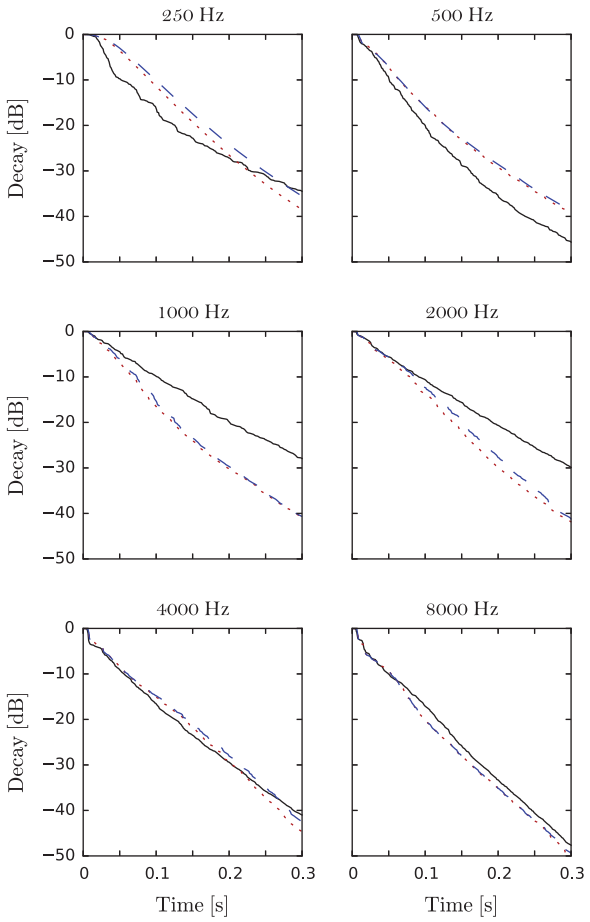

Figure 10: Decays of the empty room in receiver point P_1. *Solid black line:* Measurement, *Dotted red line:* full PARISM with 601903 image sources, *Dashed blue line:* full PARISM with 1437111 image sources.

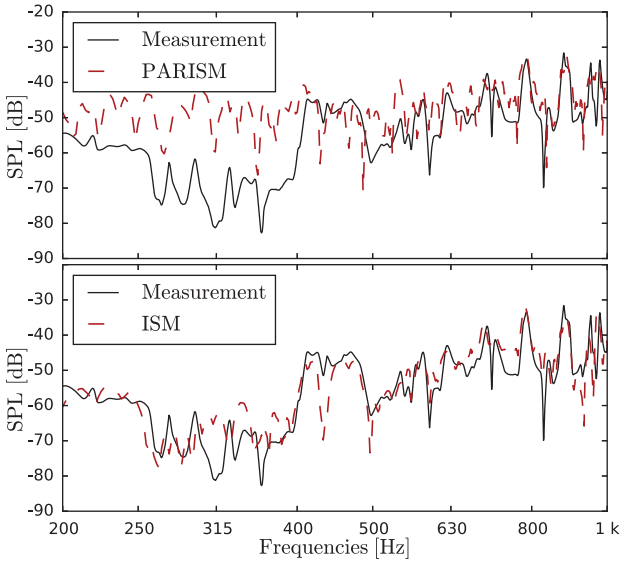

Figure 11: Measured (*solid black line*) and simulated (*dashed red line*) frequency responses of the empty room. 1120305 image sources used for the PARISM simulations. **Above:** PARISM. **Below:** Only the ISM part of the simulated response.

in this part of the model that the full frequency response is calculated, and specific peaks and dips in the response are thus found only by ISM.

There are valleys in the measured response between 250 and 500 Hz that are not matched by the PARISM response, but only by the ISM response without the AR response added. The addition of the AR response will increase the diffuseness. It is seen that there are more peaks in the PARISM response than in the ISM response below. In the shown frequency range, there are around 58 peaks in the PARISM response, around 40 in the ISM response and around 36 in the measured response. The number of peaks is thus better matched by the ISM response. It should be noted that the number of peaks is not directly related to the number of natural frequencies due to modal overlap.

The PARISM frequency responses are, as described in Sec. 3.2, calculated with a stochastic reconstruction of the AR pressure response, which means that

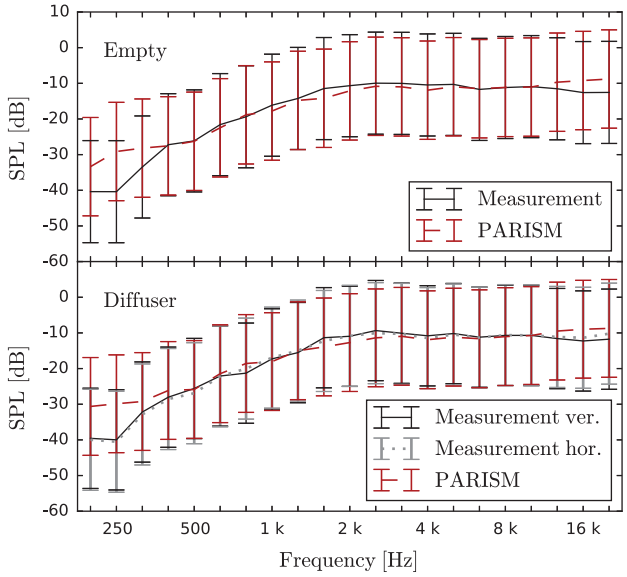

Figure 12: Spatial means and standard deviations of the 1/3-octave band energies from PARISM and the measurements.

repeating the realization will give slightly different results.

The 1/3-octave band levels are calculated for all positions, and the means and the standard deviations are taken from the squared absolute responses. These are shown in Fig. 12, where it is seen that the overall energy balance of the PARISM simulations matches the energy balance of the measurement well above around 400 Hz. The standard deviations are also matched well by the simulation.

4.4. Single reflection from the ceiling

As shown in Fig. 9, some of the decay curves of the PARISM simulations with the phased and angle-dependent ceiling reflections were more linear than the simulations with the random incidence absorption coefficient. The difference between these two simulations lies only in how the reflections from the ceiling are treated, and a single ceiling reflection is therefore regarded. The distance to the ceiling is 0.75 m, which corresponds to a first order reflection. As shown in

Eq. 2, a simple reflection model that assumes plane waves is used in PARISM, which can be problematic for sources close to the surface [9]. A reflection model of spherical waves above an impedance surface [42] was therefore compared to the simple model, and for the present case no difference was observed. The presented results are thus from the simple reflection model. Fig. 13 shows the pressure impulse response from an image source with angles 0 and 60 degrees with the ceiling. Regarding the reflection created with the reflection factor at 0 degrees in Fig. 13, it is seen that there is a peak around 0.6 ms after the first peak and that this peak is not present for the reflection created with the random incidence absorption coefficient. 0.6 s corresponds to the time it takes for sound to travel 0.2 m which is twice the distance between the surface of the absorber and the rigid backing. The calculated surface impedance thus accounts for the fact there will be reflections and resonances in the air gap. This effect is seen for the present absorber because it has a high flow resistivity. This behaviour is of course lost when the random incidence absorption coefficient is used as shown by the dashed blue line in Fig. 13. For a reflection at 60 degrees as shown in the lower part of Fig. 13, the second peak is less pronounced and the response is more similar to that of that of the random incidence absorption coefficient.

4.5. Calculation times

All simulations are carried out on a 16 GB RAM desktop computer (Dell, TX) with a 3.6 GHz processor (Intel, CA). For PARISM, the calculations took around 10 hours for a single receiver position to obtain acceptable results also at the late part of the decay. There was no significant difference in the calculation time with and without the diffuser. With the diffuser, there are 9 surfaces instead of 6 as in the empty case, but the increased scattering means that the termination of the ISM happens faster than in the empty room.

The most computationally heavy part of the PARISM simulations is the ISM. For a non-diffuse sound field such as the present, the specular reflections are of great importance and many image sources must therefore be included. In the PARISM simulations around 500 thousand image sources were included

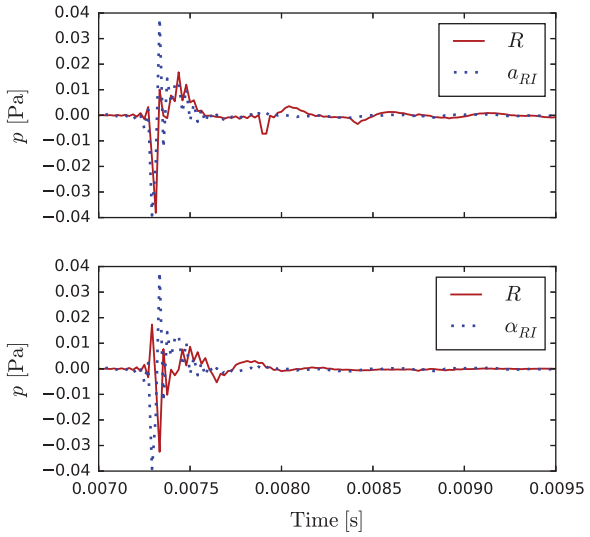

Figure 13: Single reflections from the ceiling simulated by an image source at a distance of 1.5 m. **Above:** For 0 degrees incidence angle. **Below:** For 60 degrees incidence angle. *Solid red line:* With the reflection factor, *dashed blue line:* with the random incidence absorption coefficient.

on average in the simulations, excluding the simulations with the decreased energy fraction termination criterion. For the simulation with this criterion in the empty room, the number of image sources was as mentioned 1120305 and the calculation time was nearly 25 hours.

The ODEON simulation is much faster and only takes around 3 minutes for a single receiver position, which makes ODEON far superior in terms of calculation time. It was however also shown that ODEON is not sensitive enough to frequency, position and surface scattering for simulations of the present room type.

5. Discussion

The chosen test case has proven to be a rather difficult one to simulate with phased and unphased geometrical acoustic models. Due to the very low scattering in the room and the absorbing ceiling, many specular reflections need to be included with detailed descriptions, meaning that their angles of incidence on reflecting surfaces should be included along with the phase on reflections and in propagation. This requires both a precise method and precise input data. It was shown that by including phased reflections, PARISM offers results that correspond better with the measurements than an energy-based geometrical acoustic method does, but there were still noticeable deviations between the measured results and the PARISM results.

The termination of the image source model has been pointed out as a source of the mismatch between the PARISM simulation and the measurements. It can be eliminated by adjustments in PARISM, but including a sufficient amount of image sources results in impractical calculation times. It was seen in Table 4 that the reverberation time is not sufficiently influenced by the introduction of the diffuser. This can also be linked with including too few image sources, because too few image sources can lead to the simulated sound field being too diffuse. So if the sound field is already predicted to be too diffuse in the empty room, introducing the diffuser can have too little influence.

ODEON offers very fast results, but it is also apparent that ODEON has not been developed with focus on the present room type, but rather for larger rooms with more diffuse sound fields and less absorbing surfaces. In such rooms, the precise angle dependence of the surface absorption and the modal behavior of the sound field are less important, and ODEON can in such cases give valuable predictions. For small rooms with absorbing ceilings energy-based geometrical methods are however insufficient.

For simulations of non-diffuse sound fields, it is necessary to use a precise model and thus also precise input data because the more precise a model is, the more sensitive it will be to the input data. In the present case most surface properties were estimated or measured under the assumption of a diffuse field. The absorption of the chipboard was determined by measurements that assumed that the sound field is diffuse in the room without the absorbing ceiling, and the scattering coefficient of the diffuser was determined under the same assumption. This assumption is however not entirely correct, and it is furthermore not certain that random-incidence descriptors should be used in non-diffuse sound fields. The scattering coefficient of the chipboard surfaces was estimated based on experience and fitting, but it is a difficult task because rooms with low scattering are sensitive to small changes in the scattering coefficients.

The case of an empty rectangular room with an absorbing ceiling is a difficult one to simulate, because the sound field is far from diffuse. It is however also slightly unrealistic in practice because furniture, people and other objects will increase the scattering and the absorption. This would decrease the number of image sources needed to get good results. The problem with simulating more realistic cases is however that it increases the number of unknown properties because scattering and absorption from many objects must be estimated and approximated by random incidence descriptors.

The measurements in this study showed that the orientation of a diffuser can influence the results, and such a diffuser is thus not sufficiently described by the random-incidence scattering coefficient and other descriptors are therefore necessary. As mentioned in Sec. 2, the BRDF's offer a more detailed description

of the scattering from a surface, but this is however not applicable in PARISM due to the idealized diffuse distribution pattern that is assumed in AR. Perhaps, an angle-dependence of the scattering coefficient could be included such that the size of the scattering is different for different angles of incidence, but the scattering distribution pattern remains angle-independent. Knowing the angle-dependence of the scattering coefficient however increases the demands for the measurement procedure of the scattering coefficient.

Though the example might be a difficult one to simulate, it could however be interesting as a benchmark case for comparisons of room acoustic simulation tools. The difficulty of simulating the example is also in some way due to its simplicity. It is an example of a simple geometry that needs detailed input data for the surface descriptions, and though it is slightly unrealistic due to the very low scattering, it does resemble common rooms, e.g. an office. Simulations of the same case with different methods and surface descriptors could therefore be interesting.

6. Conclusions

Room acoustic measurements of a rectangular room were compared with geometrical room acoustic simulations; one which is energy-based (ODEON), while the other includes phase shifts on specular reflections and the propagation of the specularly reflected sound (PARISM). It was found that the energy-based method was inaccurate and too insensitive in terms of frequency dependence. The results from the phased geometrical method also showed large discrepancies, and it was seen that it was sensitive to the number of specular reflections that were included. Including a large number of specular reflections in a precise model can lead to unrealistically long calculation times.

The orientation of the diffuser in the measurements was shown to influence the results, indicating that using a random-incidence scattering coefficient, as is standard in many room acoustic simulation tools, can be insufficient when the diffuser is applied in a non-diffuse sound field. It might therefore be necessary

to include angle-dependent descriptors of the surface scattering.

It can be concluded that to simulate the acoustics of a rectangular room with an absorbing ceiling and low scattering, it is necessary use a precise and sensitive model with sufficiently detailed descriptors of the surface properties. Certain and detailed input data for geometrical acoustic modeling can be difficult to obtain, which is a problem for the more sensitive models such as PARISM.

[1] K. Kuttruff, M. Schroeder, On frequency response curves in rooms. comparison of experimental, theoretical and monte carlo results for the average frequency spacing between maxima, J. Acoust. Soc. Am. 34 (1962) 76–80.

[2] B. Yousefzadeh, M. Hodgson, Energy- and wave-based beam tracing prediction of room-acoustical parameters using different boundary conditions, J. Acoust. Soc. Am. 132 (2012) 1450–1461.

[3] A. Wareing, M. Hodgson, Beam-tracing model for predicting sound fields in rooms with multilayer bounding surfaces, J. Acoust. Soc. Am. 118 (2005) 2321–2331.

[4] M. Hodgson, A. Wareing, Comparisons of predicted steady-state levels in rooms with extended- and local-reaction bounding surfaces, J. Sound Vib. 309 (2008) 167–177.

[5] C.-H. Jeong, J.-G. Ih, J. H. Rindel, An approximate treatment of reflection coefficient in the phased beam tracing method for the simulation of enclosed sound fields at medium frequencies, Appl. Acoust. 69 (2008) 601–613.

[6] R. Prislan, G. Veble, D. Svensek, Ray-trace modeling of acoustic green's function based on the semiclassical (eikonal) approximation, J. Acoust. Soc. Am. 140 (2016) 2695–2702.

[7] S. M. Dance, J. P. Roberts, B. M. Shield, Computer prediction of sound distribution in enclosed spaces using an interference pressure model, Appl. Acoust. 44 (1995) 53–65.

[8] F. P. Mechel, Improved mirror source method in room acoustics, J. Sound Vib. 256 (2002) 873–940.

[9] M. Aretz, P. Dietrich, M. Vorländer, Application of the mirror source method for low frequency sound prediction in rectangular rooms, Acta Acust. united Ac. 100 (2014) 306–319.

[10] G. Marbjerg, J. Brunskog, C.-H. Jeong, E. Nilsson, Description and validation of a combined phased acoustical radiosity and image source model for predicting sound fields in rooms, J. Acoust. Soc. Am. 138 (2015) 1457–1468.

[11] G. I. Koutsouris, J. Brunskog, C.-H. Jeong, F. Jacobsen, Combination of acoustical radiosity and the image source method, J. Acoust. Soc. Am. 133 (2013) 3963–3974.

[12] G. Marbjerg, An acoustic simulation tool for rooms with absorbing ceilings, Ph.D. thesis, Technical University of Denmark, Kgs. Lyngby (2016).

[13] G. M. Naylor, ODEON - another hybrid room acoustical model, Appl. Acoust. 38 (1992) 131–143.

[14] C. Lynge, G. Koutsouris, J. Gil, ODEON manual version 13, ODEON, Kgs. Lyngby, `https://odeon.dk/wp-content/uploads/2017/09/ODEON_Manual.pdf` (2016).

[15] X. Zeng, C. L. Christensen, J. H. Rindel, Practical methods to define scattering coefficients in a room acoustics computer model, Appl. Acoust. 67 (2006) 771–786.

[16] J. H. Rindel, Modelling the angle-dependent pressure reflection factor, Appl. Acoust. 38 (1993) 223–234.

[17] M. Hodgson, Evidence of diffuse surface reflections in rooms, J. Acoust. Soc. Am. 89 (1991) 765–771.

[18] E. Nilsson, Decay processes in rooms with non-diffuse sound fields - part I: Ceiling treatment with absorbing material, Build. Acoust. 11 (2004) 39–60.

[19] C.-H. Jeong, Guideline for adopting the local reaction assumption for porous absorbers in terms of random incidence absorption coefficients, Acta Acust. united Ac. 97 (2011) 779–790.

[20] C.-H. Jeong, G. Marbjerg, J. Brunskog, Uncertainty of input data for room acoustic simulations, in: Proc. Baltic-Nordic Acoustic Meeting, European Acoustics Association, Stockholm, 2016.

[21] ISO standard 354 - measurement of sound absorption in a reverberation room, International Organization for Standardization, Geneva, Switzerland.

[22] E. T. Paris, On the coefficient of sound-absorption measured by the reverberation method, Phil. Mag. 5 (1928) 489–497.

[23] S.-I. Thomasson, Theory and experiment on the sound absorption as function of the area, Tech. Rep. No. TRITA-TAK 8201, KTH, Stockholm, Sweden (1982).

[24] ISO standard 11654 - sound absorbers for use in buildings - rating of sound absorption, International Organization for Standardization, Geneva, Switzerland.

[25] K. Gunnarsdóttir, C.-H. Jeong, G. Marbjerg, Acoustic behavior of porous ceiling absorbers based on local and extended reaction, J. Acoust. Soc. Am. 137 (2015) 509–512.

[26] C.-H. Jeong, J. Brunskog, The equivalent incidence angle for porous absorbers backed by a hard surface, J. Acoust. Soc. Am. 134 (2013) 4590–4598.

[27] A. Richard, E. Fernandez-Grande, J. Brunskog, C.-H. Jeong, Estimation of surface impedance at oblique incidence based on sparse array processing, J. Acoust. Soc. Am. 141 (2017) 4115–4125.

[28] M. Ottink, J. Brunskog, C.-H. Jeong, E. Fernandez-Grande, P. Trojgaard, E. Tiana-Roig, *In situ* measurements of the oblique incidence sound absorption coefficient for finite sized absorbers, J. Acoust. Soc. Am. 139 (2016) 41–52.

[29] Y. Miki, Acoustical properties of porous materials - modifications of delany-bazley, J. Acoust. Soc. Jpn. 11 (1990) 19–24.

[30] T. J. Cox, B.-I. L. Dalenbäck, P. D'Antonio, J. J. Embrechts, J. Y. Jeon, E. Mommertz, M. Vorländer, A tutorial on scattering and diffusion coefficients for room acoustic surfaces, Acta Acust. united Ac. 95 (2006) 1–15.

[31] ISO standard 17497-1 - sound-scattering properties of surfaces - part 1: Measurement of the random-incidence scattering coefficient in a reverberation room, International Organization for Standardization, Geneva, Switzerland.

[32] L. Savioja, U. P. Svensson, Overview of geometrical room acoustic modeling techniques, J. Acoust. Soc. Am. 138 (2015) 708–730.

[33] E. Nilsson, Decay processes in rooms with non-diffuse sound fields. part II: Effect of irregularities, Build. Acoust. 11 (2004) 133–143.

[34] ISO standard 9631-1 - attenuation of sound during propagation outdoors - part 1: Calculation of the absorption of sound by the atmosphere, International Organization for Standardization, Geneva, Switzerland.

[35] NF EN standard 29053 - materials for acoustical applications determination of airflow resistance, International Organization for Standardization, Geneva, Switzerland.

[36] C.-H. Jeong, J. Brunskog, F. Jacobsen, Room acoustic transition time based on reflection overlap, J. Acoust. Soc. Am. 127 (2010) 2733–2736.

[37] ISO standard 3382-1 - measurement of room acoustic parameters - part 1: Performance spaces, International Organization for Standardization, Geneva, Switzerland.

[38] J. S. Bradley, Review of objective room acoustics measures and future needs, Appl. Acoust. 72 (2011) 713–720.

[39] J. S. Bradley, R. Reich, S. Norcross, A just noticeable difference in c_{50} for speech, Appl. Acoust. 58 (1999) 99–108.

[40] G. A. Soulodre, B. J. S., Subjective evaluation of new room acoustic measures, J. Acoust. Soc. Am. 98 (1995) 294–301.

[41] T. J. Cox, W. J. Davies, Y. W. Lam, The sensitivity of listeners to early sound field, Acta Acust. united Ac. 79 (1993) 27–41.

[42] S.-I. Thomasson, Reflection of waves from a point source by an impedance boundary, J. Acoust. Soc. Am. 59 (1976) 780–785.